Passive Frontal Plane Stabilization in 3D Walking

Sebastian E. Sovero[1], Cenk Oguz Saglam[2] and Katie Byl[2]

***Abstract*—This paper explores the use of a single passive design to stabilize frontal plane dynamics for 3D biped walking across a range of forward velocities and/or step lengths. Particular goals are to determine if design of sagittal plane control can be done independently from design of frontal plane stabilization mechanisms, and to explore how dynamic coupling between the two planned motions affects energetic efficiency of walking. Passive dynamic walkers have long utilized curved feet for low energy frontal plane stabilization in 3d walking, with the current design practice of matching the linearized resonance of the curvature to match a particular, steady-state walking gait to achieve stable coupled limit cycle in the 3D dynamics. However, practical legged walking systems should operate across a range of velocities and step widths. We examine aspects of the nonlinear dynamics that contribute to the energy efficiency and stability of the system through simulations. Specifically, we focus on the frontal plane dynamics and the resulting variability of time-of-return for frontal plane wobbles, as a function of impact velocity. Our decoupled analysis explains some aspects of the 3D motions; however, the actual effects on cost of transport demonstrate interesting phenomena we had not anticipated. Specifically, while a general trend of increasing cost of transport for 3D vs 2D gaits with stride time does hold in our simulations, the 3D gaits sometimes require less energy than their constrained 2D counterparts, which was a surprising and encouraging result. This work provides a promising direction for the development of practical methods to utilize control designed for planar 2D walking models on more sophisticated 3D dynamic models using little or no additional active control.**

I. INTRODUCTION

Legged robotics offer the ability to traverse terrains that are impassable to more traditional wheeled robotics. Right now. our existing walking robots do not offer both efficiency and robustness to perturbations [1]. The more traditional ZMP movement robots dynamically constrain the robot for the purpose of guaranteeing dynamic stability [2]. This does provide a conservative criteria for stability [3]. Humans are an inspiration for better energetic efficiency, as they have a mechanical cost of transport of .05 [4]. The advent of passive dynamics robots in the 1980s showed that exploiting the systems natural dynamics could yield stable walking cycles [5]. Active robots have been able to incorporate some of the energy saving mechanism of passive dynamic robots. A recent example the Cornell ranger robot which demonstrated a cost of transport of .28 in 2010 [6]. In order for legged robots to be practical, we need to lower the cost of transport of existing designs.

Control of dynamic robots constrained to the sagittal plane has been the focus of our lab[7] [8]. Our sagital walkers do not exhibit a stable limit cycle in full 3D dynamic simulations. When the robot has point feet, a yaw-roll instability emerges. Experiments based on anthropomorphic provide evidence that humans require active control to stabilize an unstable mode in the lateral direction [9]. This motivates the need to stabilize the humanoid robots in the lateral plane. Biomechanic studies have identified that humans regulate this with ankle torque[10], lateral foothold placement[9], and abduction of the hip laterally [11], [12], [13]. Several dynamic robots have utilized foot shape to stabilize the lateral direction either with yaw-roll coupling[14] or curvature [15].The yaw-roll coupling uses a similar phenomenon seen in skateboards or bicycles, in which small roll deflections induces a yaw, which then corrects the roll. The concept of curved foot walking toys has been around for over a 100 years [16]. The curvature strategy [17] [15] induces a kinematic center of rotation above the center of mass. The center of mass will oscillate as a stable pendulum with dampening provided by rolling friction and impact events. Refer to Fig1b for depiction of this system.

While there appears to be a potential trade off between stability and cost of transport [18], a robot designer should also create systems with agility or versatility [19] to navigate the complex terrains of the real world. In order to test our analysis, we make a preliminary exploration of a variety of forward speeds, stride lengths, and stride times. The reason being that our hypothesis is that stride time largely determines the amount of energy necessary to stabilize the frontal plane. The designer then selects the desired controller that reaches a state with appropriate energy satisfying an appropriate stability metric and with low cost of transport. One would then switch between controllers to select the most cost efficient but stable controller depending on the operating environment. This motivates this paper's efforts to quantify and understand the stability and energetics of curved feet walking.

II. COUPLED HYBRID SYSTEMS

A. Active Hybrid System-Sagittal Plane Dynamics

We first consider the dynamics constrained to the sagittal plane. The 5 links of the walker have 5 angles, q and 5 velocities, $\dot{q}$, meaning the sagittal state exists in $\mathbb{R}^{10}$. Note that if the foot lifts off or slips, this adds 2 positional degrees of freedom and 2 translational velocities of the robot, take the sagittal state $\mathbb{R}^{10}$. Our dynamics simulation can take into account for these extra dynamics. The sagittal states have a continuous time before impact at time t_i, where the subset i represent the step number. This is summarized below as:

$$i = 0, 1, 2, ... \in N \tag{1}$$

$$X^s(t_i) = [q\ \dot{q}]^T \in \mathbb{R}^{10} \tag{2}$$

We can numerically calculate the Poincare map, Π^s, to the next preimpact time t_i with a particular deterministic controller u_s

$$X^s(t_{i+1}) = \Pi^s(X^s(t_i), u_s) \tag{3}$$

This work is supported in part by NSF Career Award number 1255018.

[1]Sebastian E. Sovero is with the Mechanical Engineering Department at the University of California, Santa Barbara CA 93106 USA sesovero at engineering.ucsb.edu

[2]Katie Byl and Cenk Oguz Saglam are with the Department of Electrical Engineering at the University of Calfornia, Santa Barbara, CA 93106 USA saglam at ece.ucsb.edu, katiebyl at gmail.com

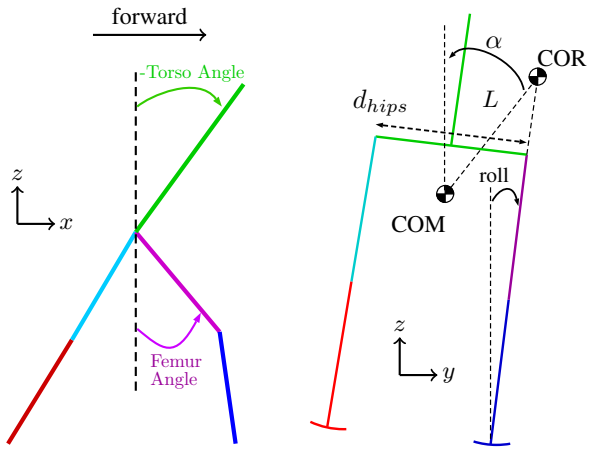

(a) sagittal plane pre impact configuration

(b) frontal plane

Fig. 1: Fig1a depicts the swing leg (on the right), just before impact. After impact the left leg will lift up and become the new swing. Our controller can regulate the torso angle, and swing femur angle at touchdown. Each foot has a Center of Rotation (COR) in Fig.1b placed directly above their respective hip. The system behaves very similarly to a stable pendulum with length L. The variable α_e is the pendulum's deflection.

We have designed a set of sagittal controllers, $U_s \in \mathbb{R}^4$, such that they each have a particular fixed point, X_d^s. The fixed point has the property:

$$X_d^s = \Pi^s(X_d^s, u_s) \tag{4}$$

This stable fixed point, X_d^s, corresponds to a particular trajectory, which we refer to as the "'gait of the robot". Two gait characteristics that we will focus on will be stride lengthλ, defined as the distance between the stance and swing foot at impact; and stride time T_s, defined as the time elapsing between impacts. We simulate the dynamics forward to develop a sagittal gait map, G^s, that take an initial condition X_0^s, and controller u_s to determine the next step's gait parameters.

$$(\lambda, T_s) = G^s(X_0^s, u_s) \tag{5}$$

B. Passive Hybrid System-Frontal Plane Dynamics

The roll dynamics are passive, and contain no active control input. We assume slipless contact is maintained by the curved foot. The Frontal states are then represented by $X^f \in \mathbb{R}^2$.

$$X^f = \begin{bmatrix} \theta_{roll} & \dot{\theta}_{roll} \end{bmatrix} \tag{6}$$

Where θ_{roll} is the body roll angle, and $\dot{\theta}_{roll}$ is the body roll speed.

The dynamics take the form of flow and impact separated:

$$X^f(t_{i+1}^-) = \Phi^f(X^f(t_i)) \tag{7}$$

$$X^f(t_{i+1}) = \Delta^f(X^f(t_{i+1}^-) \tag{8}$$

which we may take Poincare slices at the instant before impact:

$$X^f(t_{i+1}) = \Pi^f(X^f(t_i)) \tag{9}$$

Note, there exists a map of the frontal plane dynamics G^f that gives the time till next impact, T^f:

$$T^f = G^f(X^f) \tag{10}$$

As can be seen by Fig.3 G^f has an inverse map, G^{-f} defined at T_s. This would correspond to the instance when $T^f = T_s$.

$$X_*^f = G^{-f}(T^s) \tag{11}$$

For the sake of our constrained 2 dimensional frontal plane analysis we will assume that X_*^f could be a stable fixed point in the full 3D system.

C. Full 3D Dynamics

With full 3D dynamics, the frontal plane dynamics will effect the sagittal plane and visa versa. We will assume for the sake of simplified analysis that our sagittal dynamics controller will still be stable with the coupling of the frontal plane. We then introduce a coupling term C_{sf} to define the effect that sagittal plane has on the frontal plane's continuous dynamics.

$$X_d^f = \Delta^f(\Phi^f(X_d^f) + C_{sf}(X_d^f, X_d^s)) \tag{12}$$

A condition for stability:

$$\left\| \frac{\partial \Delta}{\partial X^f} \cdot \left(\frac{\partial \Phi^f}{\partial X^f} + \frac{\partial C_{sf}}{\partial X^f}\right) \right\|_\infty < 1 \tag{13}$$

which from the triangle inequality reduces to a more conservative stability condition:

$$\underbrace{\left\| \frac{\partial \Delta}{\partial X^f} \frac{\partial \Phi^f}{\partial X^f} \right\|_\infty}_{=\left\| \frac{\partial \Pi^f}{\partial X^f} \right\|_\infty} < 1 - \underbrace{\left\| \frac{\partial \Delta}{\partial X^f} \frac{\partial C_{sf}}{\partial X^f} \right\|_\infty}_{Coupling\ Term} \tag{14}$$

We equate the left half of to $\left\| \frac{\partial \Pi^f}{\partial X^f} \right\|_\infty$ -the Jacobian of the Poincare Map-usingEq.9 Eq.7 Eq.8. The right hand side is the effect of stability of the coupling term. If we assume that the coupling term is small, then the could be satisfied with:

$$\left\| \frac{\partial \Pi^f}{\partial X^f} \right\|_\infty < 1 \tag{15}$$

Since the curved foot is passive and energy normally leaves the system, Eq.15 is satisfied for a large region of X^f. Refer to Fig.2 for the actual Poincare map of the 2D Frontal Plane.

III. 2D Frontal Sway Analysis

We use the design method from [17] of matching pendulum resonance with the step frequency. Nominally, we started our design with a baseline step period of $T_s = .35s$. The curvature of the foot defines COR (center of rotation).The distance between COR and COM is called the pendulum length, L. Refer to Fig.1). We model the frontal plane simulation with all sagittal variables (i.e. joints) fixed rigidly and standing perfectly erect (similar configuration as shown in Fig.1b. This stable pendulum has a linearized period of $T_{pendulum}$ which is:

$$T_{pendulum} = (\pi)\sqrt{\frac{L}{g}} \approx .35[s] \tag{16}$$

For our design, we chose $L = 12.21$ centimeters to match our baseline gait. We do not change this parameter for any of the experiments. Our goal is to see the versatility of this fixed curvature design to different types of gaits.

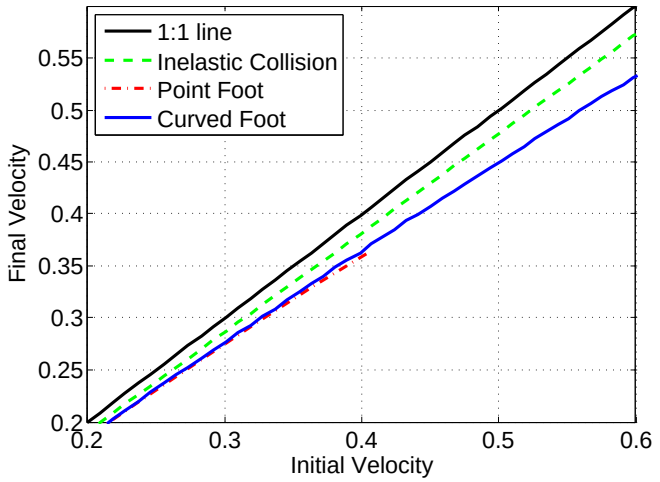

Fig. 2: $\Pi^f(X^f)$ This map looks at $\theta_{roll} = 0$ (when the impact happens). We use roll velocity state to define the map. We also simulate the point foot in the frontal plane as a comparison. Note that the Poincare map isn't defined for certain initial conditions, because the robot tips over. As expected, the point foot is stable for a smaller region. This can be seen in the figure by the red dashed line that terminates. Surprisingly the Poincare from point foot and curved foot are very similar in regards to slope.

A. Nonlinear Frontal Plane Dynamics

Note that the $T_{pendulum}$ term is derived using a small angle linearization of the full dynamics, making it an approximation. Additionally, Eq.16 also uses a point mass assumption, i.e. no rotational inertia about the center of mass. The linearization is about the equilibrium position, and the approximated system behaves like simple harmonic oscillator. However, pendulums that oscillate significantly away from the equilibrium position display nonlinear characteristics. We examined these nonlinear oscillations because we expected to drive the pendulum in nonlinear regions.

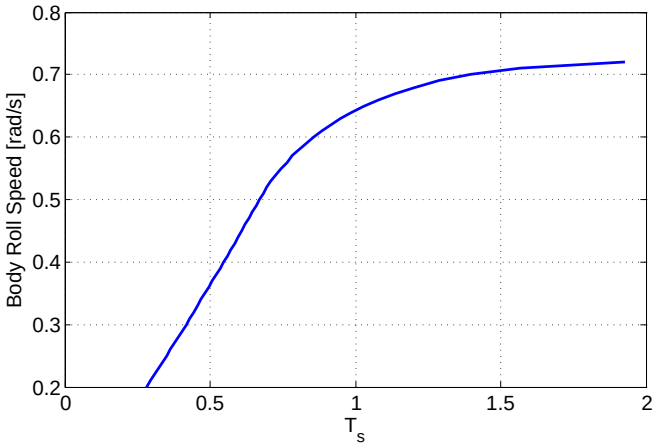

Fig. 3: G^{-f} timing map above is calculated via trajectory simulations such as those in Fig 4

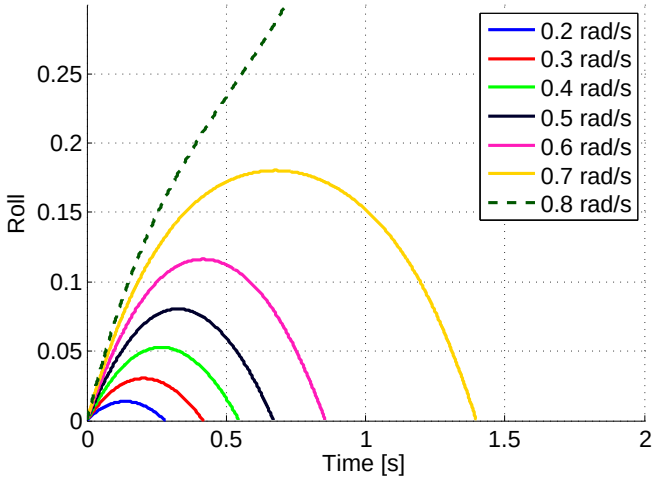

Fig. 4: To determine times of return the model was simulated with various initial roll speeds. The dashed line signifies an initial roll speed in which the robot tips over. Since this trajectory never recover to roll=0, the time return map is undefined for this velocity.

The frontal plane dynamics can be more accurately represented with pendulum length L, and rotational center of mass, I_{com}, refer to Fig.:

$$(L^2 M_t + I_{com})\ddot{\alpha} = Lsin(\alpha)M_t g \tag{17}$$

There is an offset angle between roll, $\theta_{roll}(t)$ and pendulum angle, α (refer to fig.1b):

$$\alpha(t) = \theta_{roll}(t) + \alpha_e \tag{18}$$

where α_e is an offset angle defined by the geometry as:

$$\alpha_e = sin^{-1}\left(\frac{d_{hip}}{2L}\right) \tag{19}$$

While the assumption of a linearized pendulum would make one expect a flat timing map ($T_{pendulum} = G(X^f)$ for

all X^f). Simple harmonic oscillators, which a linearized pendulum is, always have the same oscillation period regardless of initial velocity (can explained by one characteristic frequency to the homogeneous solution). The actual timing map for the nonlinear oscillator was numerically determined and is shown for the curved foot design in Fig 3. Notice that the map G^f is not defined for all roll velocities. For example, when the initial roll velocity is too high the trajectory never returns, leaving map undefined for a certain regions of X^f. Refer to Fig4 for examples.

B. 2D Curved Foot Energy Dissipation

If the solution to Eq.11, X^f_* exists and satisfies Eq.12 and Eq.13, then X^f_* is a stable fixed point. For the sake of simplified analysis, We assume Eq.12 and Eq.13 are a satisfied. This was experimentally verified by simply running the full simulation. Because X^f_* trajectory is passive, we assume the energy must flow from the sagittal to the frontal plane to keep it oscillating. We define $E_{frontal}$ as the extra energy necessary to run the 3D model compared to the 2D model over one step. We can then define a $COT_{frontal}$ as:

$$COT_{frontal} = \frac{E_{frontal}}{M_t g \lambda} \tag{20}$$

We try to approximate the energy lost in the frontal plane$E_{frontal}$ with a energy function. If we define the Total Energy Function, H as map from X_f:

$$H(X^f_i) = Kinetic + Potential = E_i \tag{21}$$

Then the energy dissipated over one cycle is approximated as:

$$\begin{aligned} E_{frontal} &= E_{i+1} - E_i \\ &= H(\Pi^f(X^f_*)) - H(X^f_*) \\ &= H(\Pi^f(G^{-f}(T_s))) - H(G^{-f}(T_s)) \end{aligned}$$

Our simplified 2D frontal plane analysis shows a prediction in Fig. 5. At this point in the analysis, we don't have specific stride length in mind so we simply plot $E_{frontal}$ as function of stride time, T_s.

IV. 2 Dimensionally Constrained Sagittal Plane Design

We used the Sliding Mode Control (SMC) framework with Time-Invariant Piece-Wise Constant References developed by Saglam and Byl[20]. Unless otherwise noted, we used the Saglam Controller parameters listed in the last column of Table 1 on page 5 of [20]. The only variables we adjusted were θ_2^{ref2}, which we will refer to as "'Femur Angle" in Fig.1a or abbreviated at "FA" in later figures for sake of brevity. The only other control parameter we adjusted was θ_5^{ref} corresponding to "Torso Angle" in Fig.1a.

We used the Saglam Controller as the basis for design, because it had been proven robust to unknown terrain variations in 2D Sagittal Walking. To test a variety of stepping gaits, we varied the "Femur Angle"and "Torso Angle" references. In general, forward leaning has been linked to faster forward speeds [21]. As can be seen in Fig.6 forward torso leaning (negative angles) successfully produces to faster walking in our model, and shrinking the Femur Angle generally shorten the step length, as would be expected from geometry.

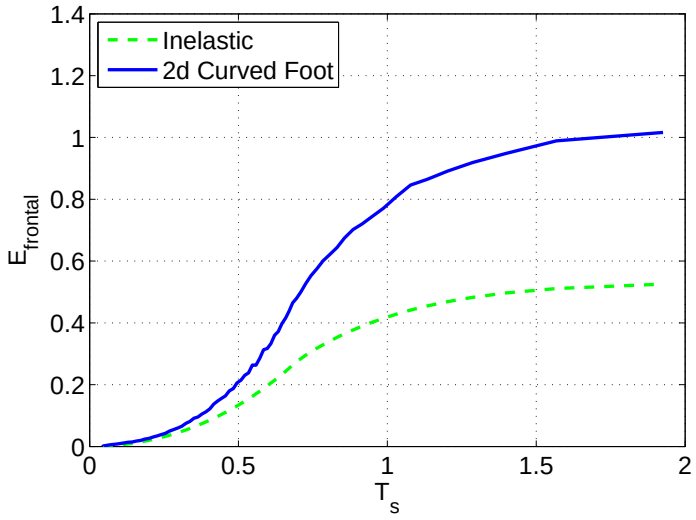

Fig. 5: The Energy units are Joules expended per time step. The energy consumption predicted by inelastic collisions does not fully explain energy loss of the 2d frontal plane system. The energy loss of the point foot system displays is slightly higher than the inelastic collision, likely due to damping introduced by rolling friction of a curved foot. Note that there is increasing trend in energy consumption with larger stride times.

The Table I succinctly summarizes the variety of forward speeds and perhaps more inspiringly, the variety of stride lengths. A variety of stride lengths enables traversal of intermittent foot holds which would be a metric for versatility of a robot. These gaits all these gaits were steady limit cycles. How quickly one could switch controllers and effect the next step length is topic of future work. Refer to Fig for the full details of gaits generated

TABLE I: Range of 2D Gaits Found

Description	Min	Max
2D Forward Speed	.6 m/s	1.6 m/s
2D Stride Time	.4 s	.65 s
2D Stride Length	.25 m	.6 m

V. Simulator and Models

For the simulations in this paper, we used the MuJoCo Physics Engine developed by Emo Todorov [22]. The model's physical parameters are the same as listed in Ref [20]. The rotational inertias of each link were considered the same in each direction. The lateral seperation of the hips, d_{hips} was 20cm. The robot was completely unconstrained in 3D space and did not have any additional actuators than we used in the 2D models.

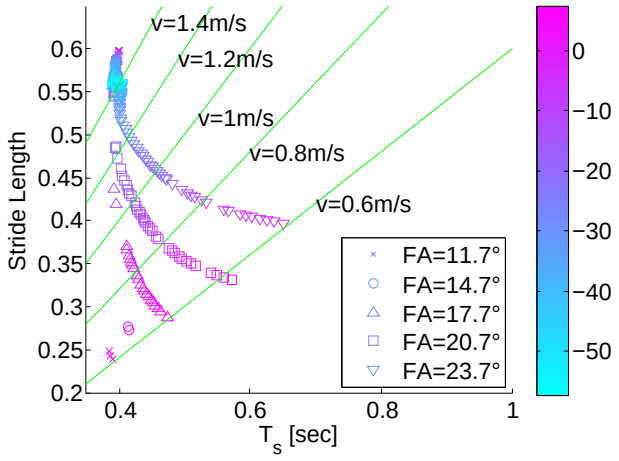

Fig. 6: Each point represents a stable gait in the sagittally constrained plane. The green lines represent constant forward speed (as labeled)in the stride length and stride time plane. The colors correspond to changes in "Torso Angle"; note negative angles mean leaning forward (refer to Fig.1a). Various FA markers correspond to the different Femur Angle. Naturally, larger femur angles extend the swing leg further creating a wider stride.

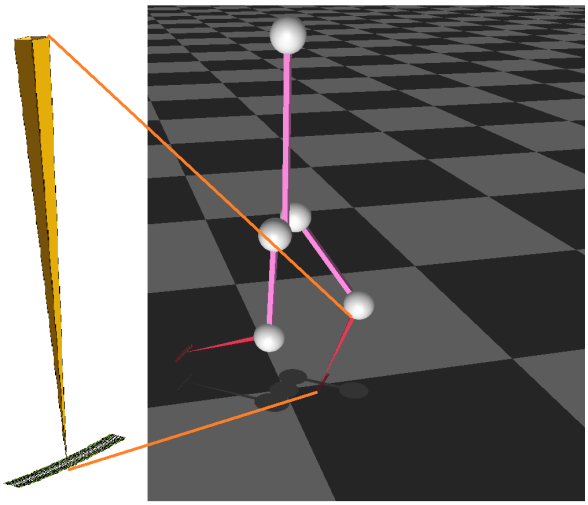

Fig. 7: The Visualization from MuJoCo Simulator is on the right. We placed a magnified view of the curved foot geometry on the left. The center of curvature 80cm above the foot, arc length of 10 °, and a width of 1.8cm

VI. Full 3 Dimensional Dynamics Simulation

A. 3D Shifting of Gait Characteristics

Predominantly, we noticed 3D gaits were shifted towards slower speeds with a few outliers. The walking speed variability was due both to changes in Stride Length (Fig.9) and Stride Time(Fig.8). We suspect that the stride was more susceptible to 3D variations because our controller enforces references dependent on phase variable, not on specific timing.

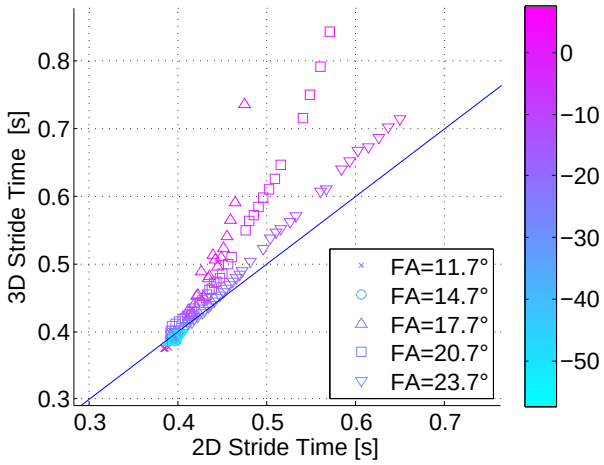

Fig. 8: Stride Time change from 2D to 3D. Color bar still represents "Torso Angle"

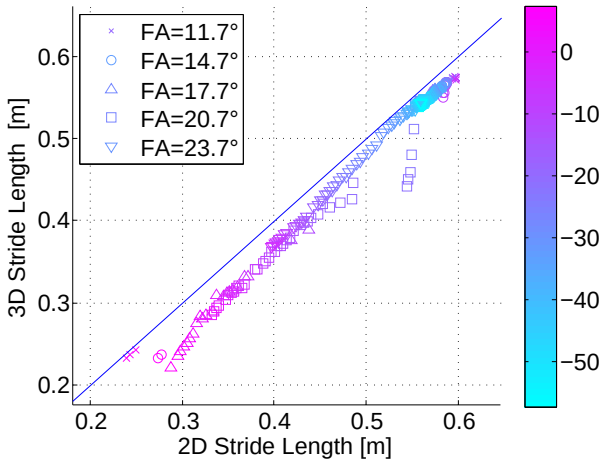

Fig. 9: Step Length change from 2D to 3D. Color bar still represents "Torso Angle"

B. Energy Consumption

We define the Mechanical Power flux, P_n at each actuator (n index 1 through 4)

$$P_n(t) = \omega_n \cdot \tau_n \tag{22}$$

We use two different work metrics for the robot. First we considered was conservative work which is the energetic worst case. Walking gaits had a high amount of variability in performance as can be seen in Fig.10, with an optimal walking speed near 1 m/s.

$$W_{conservative} = \int_0^{T_s} \sum^{n} |P_n(t)| dt \tag{23}$$

Finally, the last metric we evaluated was the Net Mechanical energy which assumes that the actuator can recover negative energy. For practical robots, actuator losses make reaching this level of energy efficiency impossible. Human metabolic cost of transport is 5 to 6 times above the mechanical cost of transport. We instead use this metric look for the increase in energy going to 3D dynamics.

$$W_{net} = \int_0^{T_s} \sum^{n} P_n(t)dt \tag{24}$$

Note as can be seen in Fig11 there was a general trend for the COT to go up at higher speeds. Generally, increases in walking speeds cause larger expenditures of energy in humans. The small decrease in energy expenditure at the end of the range is unexpected and needs further examination. The controllers were selected for their gait characteristics, not their energy efficiency. We expect 2D energy efficiency variability to also be reflected in the 3D gaits.

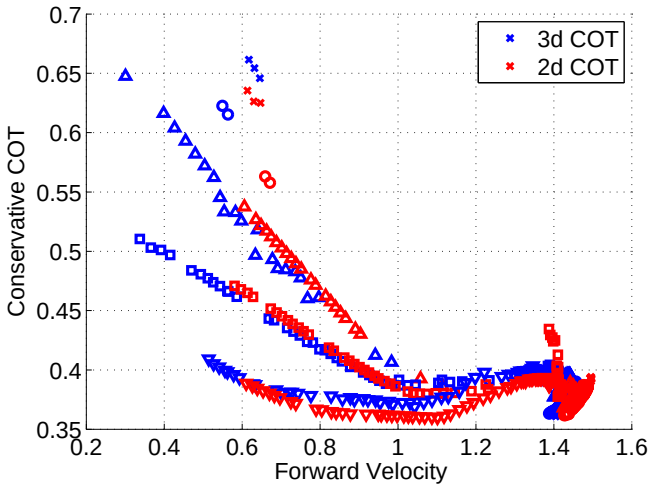

Fig. 10: This COT corresponds to the work in Eq.23. There was mixed responses of 3D gaits being more or less energy efficient.

While we studied a large number of stable gaits found in 2D and 3D walking, the $FA = 20.7$ and $FA = 23.7$ was the only data sets where 3D and 2D gaits were comparable. Parts of these data sets had minimal Stride Time and Stride Length changes from 2D to 3D. As can be seen in Fig. 12 the generally trend upheld as predicted by our analysis. Oddly, for shorter stride times, gaits actually became more energy efficient than their 2D counterparts. The exact mode of whether there is benificial energy storage in the frontal plane, or shifting of the sagittal gait into more efficient regime is yet to be determined.

VII. Future Work

Our energy assumption is based of the 2D impact map's timing function G^f. One should actually calculate a full G^{3d} which is function of the full state (sagittal, and frontal states). Preliminary investigations into the 3d frontal plane oscillations indicate a significant departure from the uncoupled dynamics.

The sagittal gait map G^s was used to characterize our gaits in this paper, but it would be interesting use it online

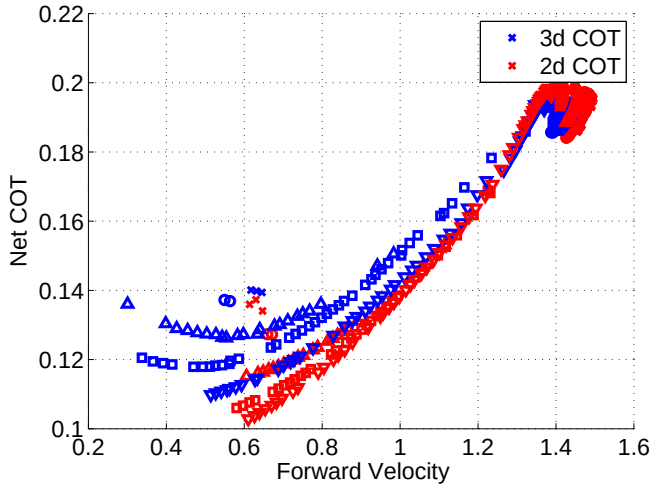

Fig. 11: Cost of Transport corresponding to Eq.24. This more generally trends with 3D gaits requiring more energy expendatures.

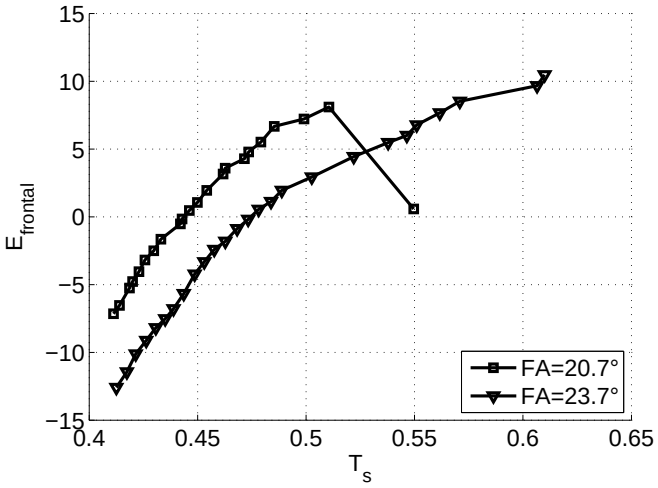

Fig. 12: Difference between 2D and 3D COT normalized by the step length λ. The data sets $FA = 20.7$ and $FA = 23.7$ had minimal changes in the sagittal planes stride length and stride time in 3d. This allowed us to more easily isolate the effect of adding frontal plane dynamics. If the sagittal plane's gait changed too significantly, we couldn't be sure if changes in energy were from the frontal plane or sagittal plane. The units of energy are joules expended during one step period.

for foothold placement selection. The computability of this map may be challenging due to the high dimensionality of the system ($\mathbb{R}^{22}$), also known at the "curse of dimensionality". We plan to see if our meshing algorithms can be used to reduce the problem's dimension to computationally feasible problem [23].

References

[1] A. D. Kuo, "Choosing your steps carefully," *Robotics & Automation Magazine, IEEE*, vol. 14, no. 2, pp. 18–29, 2007.

[2] M. Dekker, "Zero-moment point method for stable biped walking," *Internship report, Eindhoven*, 2009.

[3] A. Goswami, "Postural stability of biped robots and the foot-rotation indicator (fri) point," *The International Journal of Robotics Research*, vol. 18, no. 6, pp. 523–533, 1999.

[4] R. Margaria, "Positive and negative work performances and their efficiencies in human locomotion," *Internationale Zeitschrift für angewandte Physiologie einschließlich Arbeitsphysiologie*, vol. 25, no. 4, pp. 339–351, 1968.

[5] T. McGeer, "Passive dynamic walking," *the international journal of robotics research*, vol. 9, no. 2, pp. 62–82, 1990.

[6] P. A. Bhounsule, J. Cortell, A. Grewal, B. Hendriksen, J. D. Karssen, C. Paul, and A. Ruina, "Low-bandwidth reflex-based control for lower power walking: 65 km on a single battery charge," *The International Journal of Robotics Research*, vol. 33, no. 10, pp. 1305–1321, 2014.

[7] C. O. Saglam and K. Byl, "Stability and gait transition of the five-link biped on stochastically rough terrain using a discrete set of sliding mode controllers," in *Robotics and Automation (ICRA), 2013 IEEE International Conference on*, pp. 5675–5682, IEEE, 2013.

[8] C. O. Saglam and K. Byl, "Switching policies for metastable walking," in *Decision and Control (CDC), 2013 IEEE 52nd Annual Conference on*, pp. 977–983, IEEE, 2013.

[9] C. E. Bauby and A. D. Kuo, "Active control of lateral balance in human walking," *Journal of biomechanics*, vol. 33, no. 11, pp. 1433–1440, 2000.

[10] N. Matsusaka, "Control of the medial-lateral balance in walking," *Acta Orthopaedica*, vol. 57, no. 6, pp. 555–559, 1986.

[11] D. A. Winter, "Human balance and posture control during standing and walking," *Gait & posture*, vol. 3, no. 4, pp. 193–214, 1995.

[12] D. A. Winter, F. Prince, J. Frank, C. Powell, and K. F. Zabjek, "Unified theory regarding a/p and m/l balance in quiet stance," *Journal of neurophysiology*, vol. 75, no. 6, pp. 2334–2343, 1996.

[13] C. D. MacKinnon and D. A. Winter, "Control of whole body balance in the frontal plane during human walking," *Journal of biomechanics*, vol. 26, no. 6, pp. 633–644, 1993.

[14] M. Wisse, "Three additions to passive dynamic walking: actuation, an upper body, and 3d stability," *International Journal of Humanoid Robotics*, vol. 2, no. 04, pp. 459–478, 2005.

[15] S. H. Collins, M. Wisse, and A. Ruina, "A three-dimensional passive-dynamic walking robot with two legs and knees," *The International Journal of Robotics Research*, vol. 20, no. 7, pp. 607–615, 2001.

[16] B. Bechstein, "Improvements in and relating to toys," *UK Patent*, no. 7453, 1912.

[17] R. Tedrake, T. W. Zhang, M.-f. Fong, and H. S. Seung, "Actuating a simple 3d passive dynamic walker," in *Robotics and Automation, 2004. Proceedings. ICRA'04. 2004 IEEE International Conference on*, vol. 5, pp. 4656–4661, IEEE, 2004.

[18] C. O. Saglam and K. Byl, "Quantifying the trade-offs between stability versus energy use for underactuated biped walking,"

[19] D. G. Hobbelen and M. Wisse, *Limit cycle walking*. na, 2007.

[20] C. O. Saglam and K. Byl, "Quantifying and optimizing stability of bipedal walking gaits," in *IEEE International Conference on Robotics and Automation (ICRA)*, 2015. submitted.

[21] M.-Y. Chen and K. Byl, "Analysis and control techniques for the compass gait with a torso walking on stochastically rough terrain," in *American Control Conference (ACC), 2012*, pp. 3451–3458, IEEE, 2012.

[22] E. Todorov, T. Erez, and Y. Tassa, "Mujoco: A physics engine for model-based control," in *IEEE Int. Conf. on Intel. Robots and Systems (IROS)*, pp. 5026–5033, 2012.

[23] C. O. Saglam and K. Byl, "Robust policies via meshing for metastable rough terrain walking," RSS, 2014.